DOE/ER/45237-T1

PERFORMANCE REPORT (4/1/89-10/25/89)

by
Benjamin Chu
Department of Chemistry
State University of New York at Stony Brook
Long Island, New York 11794-3400

DOE/ER/45237--T1

DE90 003525

Title: Phase Transition in Polymer Blends and Structure of Ionomers

Award Period: 4/1/89 - 3/31/90

Award Amount: $100,000

Sponsor ID: DEFG0286ER45237

During the first year of this award period, the SUNY X3A2 Beamline experienced problems due to x-ray mirror damage, the departure of the Beamline Coordinator, Dr. J. Phillips, and a switch of the X3A2 geometry. The departure of the Beamline Coordinator resulted in reformulation of beamline upkeep procedures. The operational problems are being smoothed out. The damaged x-ray mirror prevented us from making scattering measurements at very small angles ($\lesssim$ 1.5 milliradian). It may be anticipated that the mirror will be optimized for anomalous x-ray diffraction measurements, but not for SAXS. So, we plan to make further modifications by adding an additional slit collimation setup in our SAXS apparatus.

With the SUNY beamline moving from X-21 to X-3, modification of the A2 port instrumentation configuration switched the position of the large Huber x-ray diffractometer with that of the Kratky SAXS diffractometer, i.e., the synchrotron x-ray beam first reaches the SAXS diffractometer before it becomes available to the x-ray diffractometer as shown in Fig. 1. The switch permits the x-ray diffractometer to perform anomalous x-ray diffraction of high T_c superconductor crystals but requires the removal of the entire small angle x-ray scattering instrumentation from the hutch after each use. In the first two periods for SAXS experiments, the SAXS instrumentation had to be stored in a separate building after each use. This arrangement was completely

do

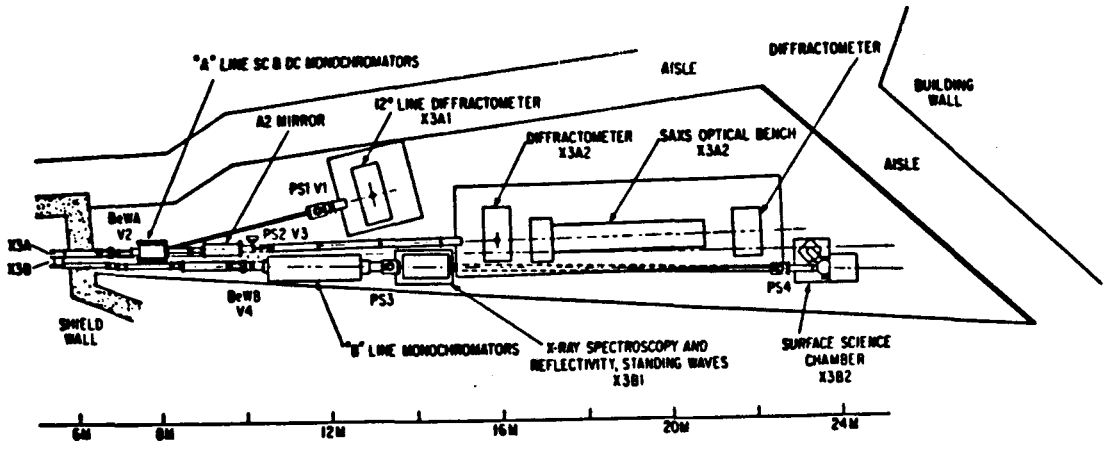

FIGURE 1. *The SUNY X3 Beamline at NSLS*

unsatisfactory, as moving the SAXS diffractometer required partial disassembly and invariably introduced vibrations in transit. The result was a serious misalignment of the SAXS diffractometer after the second move, involving possible damage to one of the fine (θ/ϕ) adjustments for the Kratky slit collimator. Realignment time increased after each move.

The difficulty is being alleviated temporarily by designing a rail system for the optical bench which holds the SAXS diffractometer. If the rail system is installed in time, the Kratky SAXS diffractometer could be moved to the side after use without disassembly starting from the next SAXS run. This arrangement remains a compromise, as in principle, it is never a good practice to move major instrumentation, especially during the developmental stage. The best arrangement remains that the large x-ray diffractor should be in front of the SAXS instrumentation so that both instruments do not move after use. This problem remains to be resolved.

With the above handicap, which has involved extensive time for SAXS instrument alignment, we report our activities as follows.

I. Conference and Seminar Activities

II. Publications

III. Summary of Experiments Performed

IV. Proposed Studies

I. Conference and Seminar Activities

1988. 1. NATO ASI on Reactive and Flexible Molecules in Liquids, Nauplia, Greece. "Structure and Dynamics of Branched (Epoxy) Polymers and Kinetics of the Polymerization Process," (2 lectures) by B. Chu and C. Wu. (B. Chu, Invited speaker and session chairman).

2. Materials Research Society; Symposium V: Synchrotron Radiation in Materials Research, Boston, MA. "Time-Resolved Small Angle X-Ray Scattering and Dynamic Light Scattering Studies of Sol-Gel Transition of Gelatin," by D.-Q. Wu and B. Chu. (Paper presented by D.-Q. Wu).

1989. 3. Rolduc Polymer Meeting 4, Limburg, The Netherlands. "Branching Kinetics of Epoxy Polymerization of 1,4-Butanediol Diglycidyl Ether with Cis-1,2-Cyclohexanedicarboxylic Anhydride," by B. Chu and C. Wu. (Talk presented).

4. 1989 NSLS Annual User's Meeting, Brookhaven National Lab, Upton, New York. Posters presented:

   1) Evaluation of a Photo-diode Array Detector for Small Angle X-Ray Scattering Measurements, by B. Chu, D. Q. Wu and R. Howard.

   2) Developments on a CCD Two-Dimensional X-Ray Detector, by H. F. Fuchs, D. Q. Wu and B. Chu.

   3) Small Angle X-Ray Scattering on Poly(ethylene-methacrylic Acid)/Pb and PbS Ionomers, by B. Chu, D. Q. Wu, J. C. Phillips and W. Mahler.

   4) Small Angle X-Ray Scattering Studies of Sulfonated Polystyrene Ionomers: Temperature Effect, by D. Q. Wu, J. C. Phillips, R. Lundberg, W. MacKnight and B. Chu.

   5) Synchrotron SAXS Measurements on Solutions of Poly(styrene-isoprene) AB Block Copolymer in Aniline, by R. Hilfiker, D. Q. Wu, J. C. Phillips and B. Chu.

   6) Structure and Dynamics of Gelatin in Sol and in Gel, by D. Q. Wu, M. Djabourov, J. Leblond, J. C. Phillips and B. Chu.

   7) Simultaneous Small Angle and Wide Angle X-Ray Scattering on Crystallization of Polyethylene Blends, by B. Chu, D. Q. Wu, M. Satkowski, S. McGuire, R. S. Stein and J. C. Phillips.

8) Synchrotron X-Ray Diffraction of a Single Filament and Bundles of Poly(p-phenylene terepthalamide) Fibers, by B. Chu, C. Wu, Y. J. Li, G. S. Harbison, E. J. Roche, S. R. Allen, T. F. McNulty and J. C. Phillips.

9) High Flux X-Ray Scattering of Polydiacetylene (P4BCMU) in Dilute Toluene Solution, by B. Chu, R. Xu, Y. J. Li, D. Q. Wu and J. C. Phillips.

II. Publications

1. Pei Tang, David E. Colflesh and Benjamin Chu, "Temperature Effect on Fractal Structure of Silica Aggregates," *J. Colloid and Interface Sci.*, **126**, 304 (1988).
2. Benjamin Chu, Renliang Xu, Zhulun Wang and Ju Zuo, "Critical Phenomena and Polymer Coil-to-Globule Transition," *J. Appl. Cryst.*, **21**, 707 (1988).
3. D. W. Schaefer, C. J. Brinker, J. P. Wilcoxon, D. Q. Wu, J. C. Phillips and B. Chu, "Precursor Chemistry and the Structure of Silica Aerogels," in Proceedings of the Materials Research Society Symposium, **Vol. 121**, *Better Ceramics Through Chemistry III*, C. J. Brinker, D. E. Clark and D. R. Ulrich, eds. (1988) pp. 691-696.
4. Benjamin Chu, "Small Angle X-Ray Scattering Studies of Sulfonated Polystyrene Ionomers" in Proceedings of the 19th Yamada Conference on Ordering and Organization in Ionic Solutions, eds. N. Ise and I. Sogami, World Scientific Publishing Co., Pte. Ltd., Singapore and Yamada Science Foundation, Osaka (1988), pp. 67-81.
5. D.-Q. Wu, J. C. Phillips, R. D. Lundberg, W. J. MacKnight and B. Chu, "Long Range Inhomogeneity of Sulfonated Polystyrene Ionomers," *Macromolecules*, Note, **22**, 992 (1989).
6. Dan Q. Wu and Benjamin Chu, "Time-Resolved Small Angle X-Ray Scattering and Dynamic Light Scattering Studies of Sol-Gel Transition of Gelatin," in Proceedings of the Materials Research Society; Symposium V: Synchrotron Radiation in Materials Research, **Vol. 143** (1989) pp. 203-208.
7. Benjamin Chu, Dan Q. Wu and Roy Howard, "Evaluation of a Linear Photodiode Array Detector for Synchrotron SAXS Measurements," *Rev. Sci. Instrum.*, **60**, 3224 (1989).

8. Rolf Hilfiker, Dan Q. Wu and Benjamin Chu, "Synchroton SAXS Measurements on Solutions of Poly(styrene-isoprene) AB Block Copolymer in Aniline," *J. Coll. & Interface Sci.*, accepted for publication.
9. H. H. Song, D. Q. Wu, B. Chu, M. Satkowski, M. Ree, R. S. Stein and J. C. Phillips, "Morphology of HDPE/LDPE Blends as Studied by Time-Resolved SAXS," *Macromolecules*, accepted for publication.
10. Heribert F. Fuchs, Dan Q. Wu and Benjamin Chu, "An Area X-Ray Detector System Based on a Commercially Available CCD-Unit," *Rev. Sci. Instrum.*, accepted for publication as a Note.

III. Summary of Experiments Performed (October 3, 1988 - March 29, 1989)*

During the past year, B. Chu and his research group continued experimental activities in the following directions.

III.A. X-Ray Detector Development

Although the SUNY Beamline has a Braun (wire) linear position sensitive detector and a Princeton Applied Research (PAR) photodiode array detector, the Braun detector cannot accept high count rates and the photodiode array detector has low counting efficiency. Furthermore, the photodiode array chip has been damaged by the intense synchrotron x-rays. As we had no funds to purchase another position sensitive detector, arrangements were made with Dr. Roy Howard at EG&G PAR to loan us an intensified photodiode array detector so that we, in collaboration with Dr. Howard, can develop a SAXS detector originally designed for visible light applications. The following shows an abstract, a figure (III.A.1), a scheme of detector operation and the detector parameters we were able to achieve. As a result of this study, we propose to modify the SUNY Beamline photodiode array detector so that we can have a modern x-ray detector for high scattered intensity and time-resolved SAXS experiments (see proposed budget).

---

* Total operating time was 25 days in 1988 (10/3-9, 10/14-19, 10/22-27, 12/17-22) and 13 days in 1989 (3/10-12, 3/17-21, 3/24-27, 3/29).

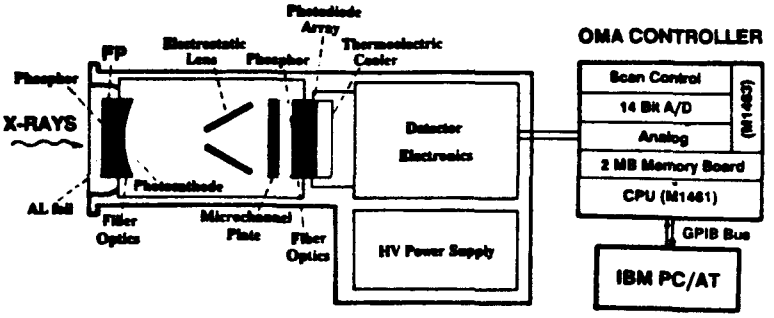

FIGURE III.A.1. *Photo-diode Array Detector for Synchrotron SAXS*

Scheme of Detector Operation

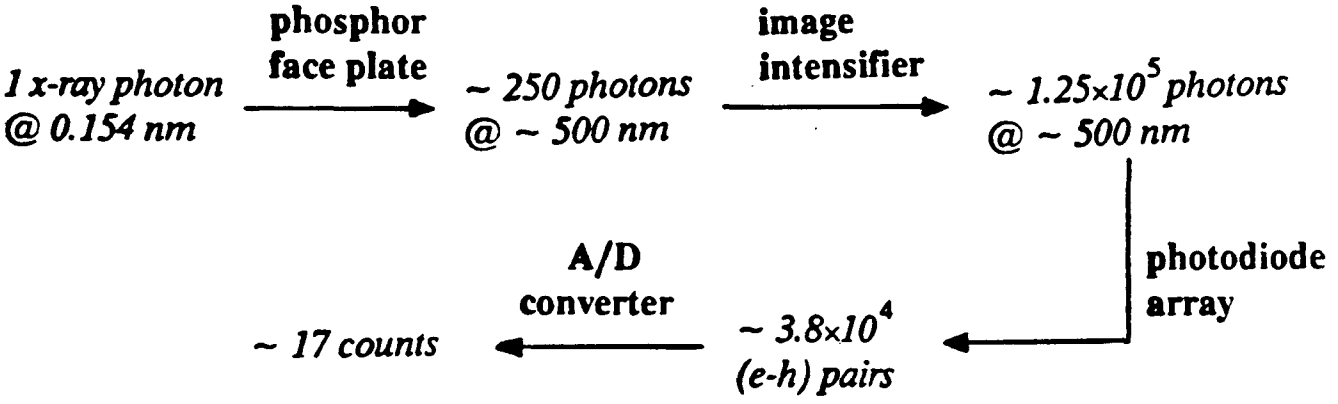

Detector Parameters

Gain: *~ 3.8×10^4 (e-h) pairs ≈ 17 counts per x-ray photon @ 0.154 nm.*

Compare to

900 - 1300 (e-h) pairs if using Direct Exposure Method

~ 110 (e-h) pairs if using Phosphor but without Intensifier

Dark Count: *~ 40 counts per pixel per second if PDA is cooled at -25 °C.*

Using an intensifier greatly enhances the signal-to-noise ratio.

Minimum Exposure Time: *16 ms*

Maximum Count Rate: *~ 6×10^4 x-rays/pixel/sec ~ 9.5×10^7 x-rays/cm^2/sec (can be increased by reducing* **Gain***.)*

Maximum Dynamic Range: *~500 (can be increased by reducing* **Gain** *)*

Detector Quantum Efficiency (DQE): DQE *~ 1 if S/N ≳ 5%*

Spatial Uniformity of Response: *± 5% mean, correctable.*

Linearity of Response vs. Intensity:

within ± 1% for ~3000 - ~5 counts/pixel/sec.

Spatial Resolution: *FWHM of the point spread function ~3-4 pixels.*

Position Linearity: *± 1 pixel per 100 pixels.*

Other Properties:

No radiation damage was observed after exposure to a main beam of 10^{10} x-ray photons/mm^2/sec for a few seconds.

The detector showed a finite afterglow time of ~5 sec due to the intensifier phosphor.

III.A.1. Evaluation of a Photo-diode Array Detector for Small Angle X-ray Scattering Measurements

A linear photodiode array detector for synchrotron SAXS was constructed by coupling a fiber-optic face plate deposited with a thin layer (~40μ) of phosphor (Y_2O_2S:Tb) onto an intensified photodiode array (EG&G, PARC Model 1422) originally designed for visible light applications. The evaluation of the detector showed excellent linearity of response to the incident x-ray intensity (< 1%), stable pixel uniformity (± 5% mean), good spatial linearity (±1 per 100 pixels), and a net gain of ~17 counts/x-ray photon @ 8KeV. The detector performed nearly ideally (DQE~1) for S/N $\gtrsim$ 5%. No damage on the pixels was found after exposure to a main beam of ~10^{10} x-rays/mm^2/sec for a few sec. The detector would be perfect for time-resolved SAXS measurement if the intensifier were replaced with the one using a fast-decay phosphor. Using a 2:1 taper instead of a 1:1 face plate would increase the effective detection length from 1 inch to 2 inches.

III.B. SAXS Experiments

In SAXS experiments, we performed measurements as a member of the PRT and with collaborators as general users in three separate modes: the collaborators handed us the samples and we did the experiments; the collaborators prepared the samples and came to NSLS to help us perform the experiments; the collaborators worked together with us in both sample preparations and in performing the experiments. We did experiments on (1) vesicle formation by block copolymers, (2) temperature effect of sulfonated polystyrene ionomers, (3) structure and dynamics of gelatin in sol and in gel.

III.B.1. Synchrotron SAXS Measurements on Solutions of Poly(styrene-isoprene) AB Block Copolymer in Aniline.

Synchrotron small angle x-ray scattering (SAXS) has been performed on solutions of a poly(styrene-isoprene) AB block (PS/PIP) copolymer in aniline. The copolymer forms aggregates as aniline is a poor solvent for PIP block. To determine whether the aggregates were micelle-like or vesicle-like, the form factor over a wide q-range was obtained with a sufficient precision. The measurement showed that the aggregates were vesicle-like when the PS block was sufficiently short. The effect of polydispersity on the form factor was also taken into account.

Experiment Conditions

Solution concentration: $8.62 \times 10^{-3}\ g/cm^3$

Instrument: *A SAXD at SUNY Beamline, using a modified Kratky slit-collimator and a BRAUN Linear Position Sensitive Detector*

X-ray wavelength: *1.54 Å*

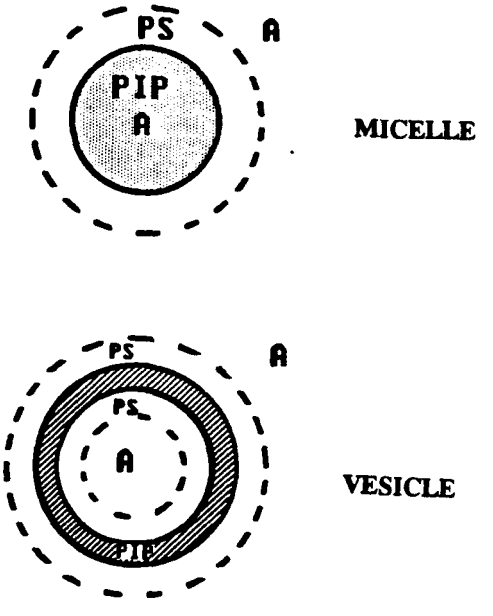

FIGURE III.B.1.1. *Schematic representation of a* **MICELLE** *and a* **VESICLE.** *Solid lines denote sharp boundaries and broken lines denote diffuse boundaries.* **PIP:** *polyisoprene;* **PS:** *polystyrene;* **A:** *aniline.*

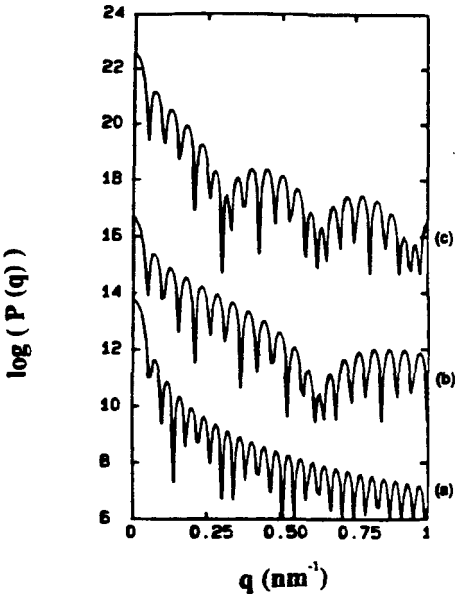

FIGURE III.B.1.2. *Logarithm of the form factor (***P(q)***)(multiplied by an arbitrary number) as a function of q[= (4π/λ)sin(θ/2), with λ and θ being the x-ray wavelength and the scattering angle, respectively]. Curve* **(a)** *is* **P(q)** *of a hard sphere with* **R** *= 77.5 nm; curves* **(b)** *and* **(c)** *are* **P(q)** *of hollow spheres with outer radius* $\mathbf{R_o}$ *= 64.7 and 68.8 and inner radius* $\mathbf{R_i}$ *= 54.7 and 48.8 nm, respectively. All three spheres have a radius of gyration of 60.0 nm.*

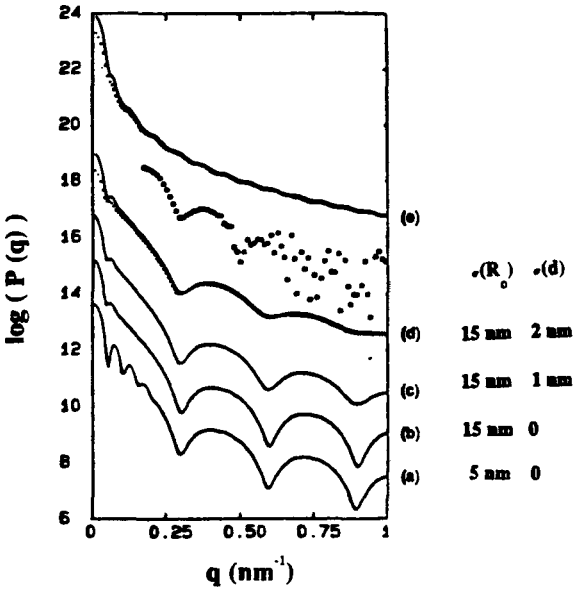

FIGURE III.B.1.3. *Logarithm of the form factor (multiplied by an arbitrary number) as a function of q. Curves* **(a)** *to* **(d)** *are form factors of hollow spheres with a mean outer radius* $\mathbf{R_o}$ *= 69 nm and a mean shell thickness* **d** *= 21 nm. Curve* **(e)** *is the form factor of a solid sphere with a mean radius* **R** *= 77.5 and σ(***R***) = 15 nm. The dotted lines show the effect of smearing due to the finite slit height. The hollow squares are the experimental data. The possibility of having a* **MICELLE** *structure is excluded. The* **VESICLE** *structure would be more reasonable.*

III.B.2. SAXS Studies of Sulfonated Polystyrene Ionomers: Temperature Effect.

The study aims at a full understanding on the ionomer morphology, especially the spatial arrangement of ions in ionomers. Small angle x-ray scattering (SAXS) measurements on a model system: sulfonated polystyrene (SPS) sodium and zinc salts, have revealed new structural information. The SAXS profiles with a wide angular range, a high spatial resolution and a good precision have shown that the existing models for the structure of ionic aggregates would not work well: an inter-particle interference model (or liquid-like model) could not explain the small angle upturn, while an intra-particle interference model (or core-shell model) could not predict an ion cluster "size" of ~20 nm.

It is known that the ionic aggregation is responsible for many improved mechanical properties, such as an increase in the glass transition temperature, T_g and in storage modulus. The SAXS experiments of 4.3 mol% SPS Na and Zn salts at elevated temperatures above T_g agreed well with the findings of the viscoelastic measurements.

Figures III.B.2.1 and III.B.2.2 showed that SAXS patterns of SPS-Na and SPS-Zn salts, respectively. An ionic peak was observed for all ionomer samples even at 250°C. Upon being heated to at least ~200°C, an increase in the ionic peak height and peak width suggested that more ion pairs would have aggregated to form small clusters. The Na and Zn salts demonstrated different thermal properties at 250°C. The Na salt showed a further increase in ionic peak height while the Zn salt showed a decrease in height but an increase in width. A decrease in the ionic peak height might be explained as breaking down of some ionic clusters because of thermal energy. Figure III.B.2.3 showed that the storage modulus increased with temperature from ~150°C to ~175°C (Zn) or 220°C (Na).

Data analysis on anomalous SAXS measurements and development of a new correlation function scheme are underway.

III.B.3. Structure and Dynamics of Gelatin in Sol and in Gel.

Structural and dynamic properties of aqueous gelatin solutions in a sol-gel transition were studied by small angle x-ray scattering (SAXS) and dynamic light scattering (DLS). SAXS showed an increase in scattered intensity during gelatin gelation

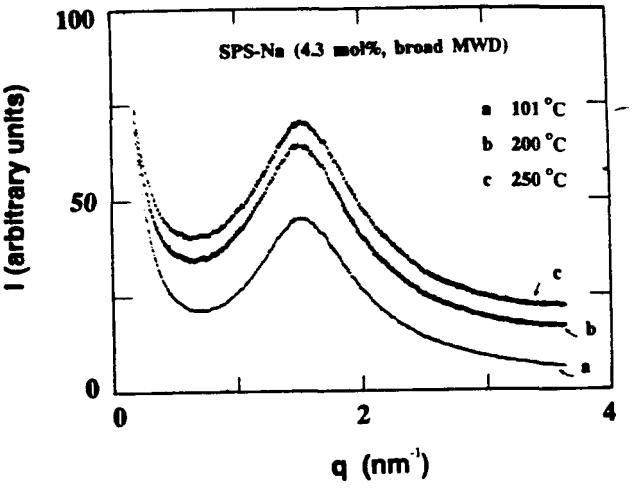

FIGURE III.B.2.1. *SAXS profiles for sodium salt of 4.3 mol % SPS with a broad MWD at three temperatures. At least an half hour was kept at each temperature. Subtraction of PS or SPS-H was not performed. The sample showed a growth of the ionic peak height and width with increasing temperature even up to 250 °C.*

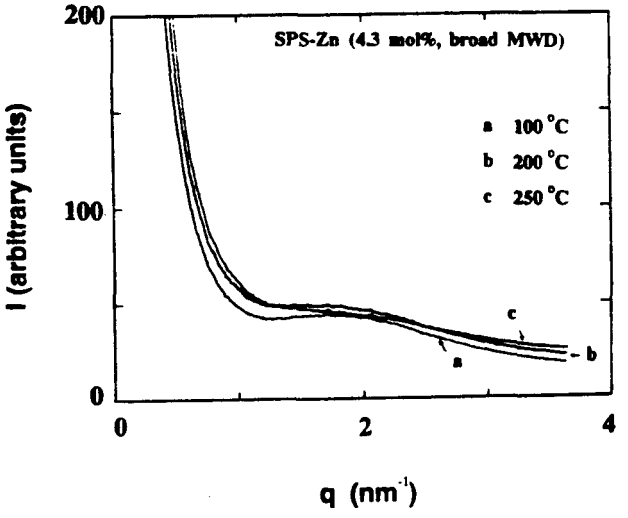

FIGURE III.B.2.2. *SAXS profiles of zinc salt of 4.3 mol % SPS with a broad MWD at three temperatures. At least an half hour was kept at each temperature. Subtraction of PS or SPS-H was not performed. The sample showed a similar change to the narrow MWD zinc salt in the ionic peak height and width. However, the amplitude of change was smaller and a much stronger zero order scattering at small angles (a larger upturn) and a less sharp ionic peak than that of the narrow MWD zinc salt was observed.*

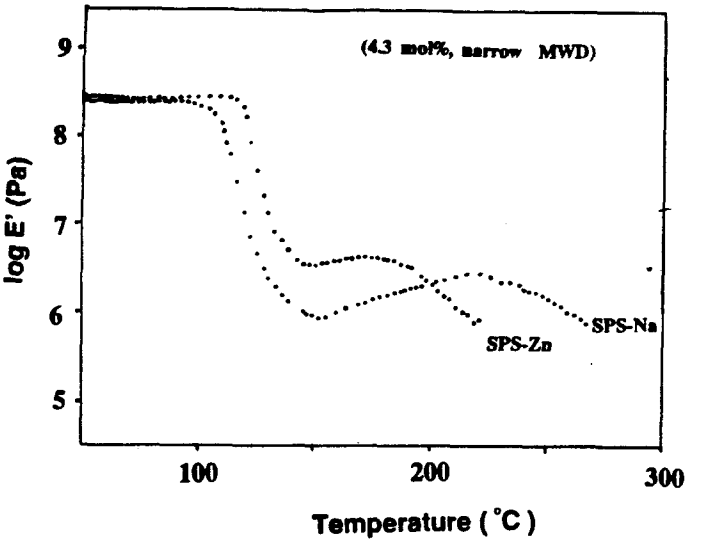

FIGURE III.B.2.3. *Storage modulus E' vs. temperature for sodium and zinc salts of 4.3 mol % SPS with a narrow MWD. After β relaxation (T≥150 °C), the sodium salt showed a large increase in storage modulus upto to ~220 °C while the zinc salt also showed an increase up to ~180 °C. A decrease in storage modulus subsequently occurred. The increase of storage modulus is an indication of an increase in cross-linking density. Here it implies probably an increase in ionic aggregates in the ionomer samples.*

that could be attributed to the aggregation of gelatin chains. When quenching a 5 wt% gelatin from ~45 °C to 11 °C, the gelatin aggregates might be in the form of fibrils which grew initially in cross-section. Gelation might follow different kinetics for a gelatin higher and lower than 5 wt%. Photon correlation, on the other hand, clearly showed two relaxation modes in the sol and near the gel point: a fast cooperative diffusion mode which remained constant from sol to gel state after correction for the temperature dependence of solvent viscosity; a slow mode, that could be originated from the self-diffusion of "free" gelatin chains and aggregates. The slow mode contribution to the intensity correlation function was reduced in the gelation process signaling a decrease but not the elimination of "free" particles in the gel network. A drastic broadening in the characteristic line-width distribution was observed.

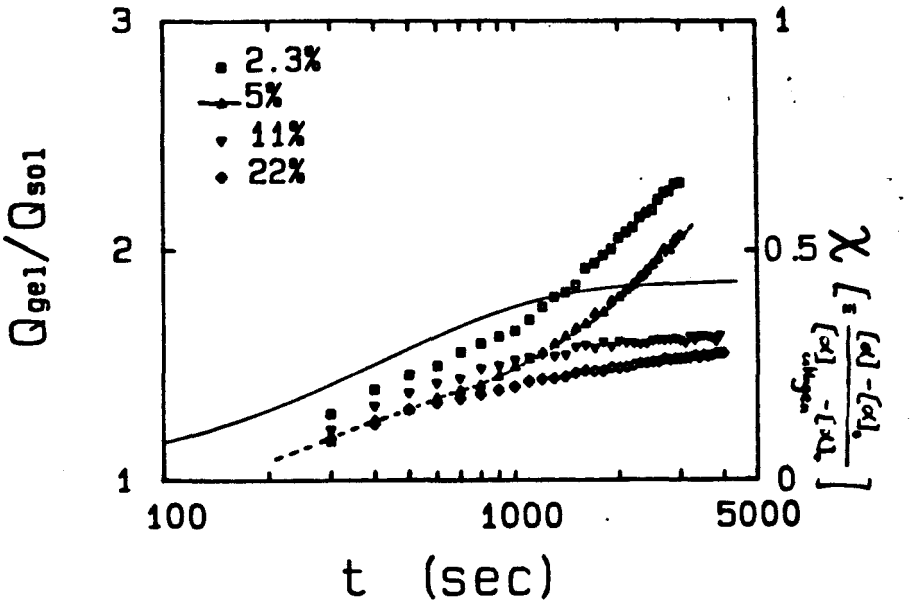

FIGURE III.B.3.1. *Normalized integrated scattered intensity of gelation solutions (0.1M NaCl, pH=7) in a sol-gel transition (quenched from ~45 °C to 11 °C). The solid line represents the coil-to-helix conversion of 5 wt% gelatin undergoing the same gelation that was measured by polarimetry)Djabourov et. at., Brit. Polym. J. 17, 169 (1986)). A profound difference in curve shape is shown between the samples of 2.3% and 5% and those of 11% and 22% suggesting a different gelation kinetics. As polarimetry measures amount of the triple helices formed, the samples of 2% and 5% might have additional aggregation other than formation of triple helices while the samples of 11% and 22% might form helices only because the gelatin chains are highly entangled.*

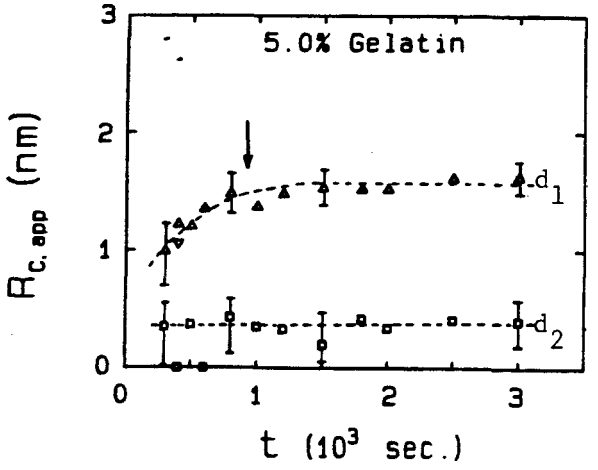

FIGURE III.B.3.2. *Plots of estimates on apparent averaged radius of gyration of the gel fibrillar cross-section vs. gelation time. The arrow points roughly at the time when three dimensional gel network was formed. The gel fibrils grew in diameter initially. An averaged maximum diameter of the fibrils* $\mathbf{d}_1$ *~ 2 nm; 2* $\mathbf{R}_{c,app}$ *~ 4.5 nm. A different size of fibrils had* $\mathbf{d}_2$ *~ 1 nm, which was close to the diameter of a triple helix.*

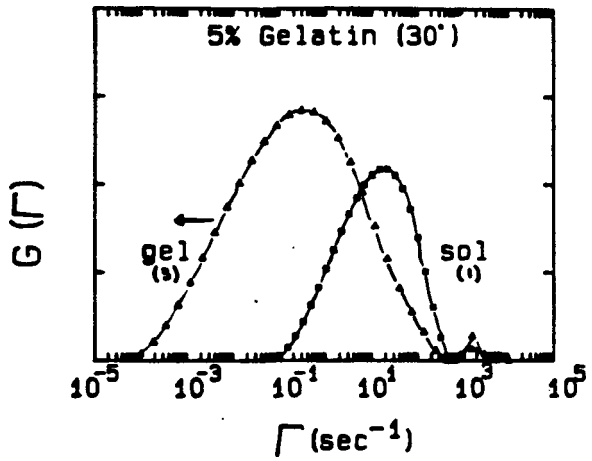

FIGURE III.B.3.3. *Typical plots of characteristic linewidth distributions of the gelatin solution based on curves 1 (sol) and 3 (gel). The peak of fast mode represents a fast cooperative diffusion diffusion because of the local gelatin concentration fluctuation while the broad peak of slow mode could be attributed to a slow self-diffusion of the "free" molecules (single chains and individual helices etc.) of the polydispersed gelatin system.*

Table I. CONTIN ANALYSIS RESULTS

	D_{slow}	A_{slow}	V_{slow}	D_{fast}	A_{fast}	V_{fast}	D_3	A_3	V_3	η(cp)
sol	1.7±0.2	0.36	0.6	50±3	0.53	0.06	12±4	0.10	0.07	0.58
gel	0.5±0.3	0.17	1.0	25±5	0.75	0.05	0.1±0.04	0.08	0.09	1.27

D: 10^{-8} cm^2/sec; $A_{slow} + A_{fast} + A_3 = 1$, typically $\Delta A = \pm 0.03$; *V*: variance of the peak in $G(\Gamma)$; η: viscosity of water at 46°C and 11°C.

IV. PROPOSED STUDIES

In the proposed studies, we hope to continue our development of SAXS instrumentation for the SUNY Beamline so that our SAXS capabilities remain a world-class facility, capable of competing with the best and at times become the best such facility for SAXS. As measurements of anisotropic systems require an area detector. The PI received a URI award on a SAXS facility from DOE. Plans have been made to incorporate the SAXS facility at Stony Brook with the SAXS instrumentation at the

SUNY X3-A2 Beamline so that at least some of the instruments can be made to become interchangeable.

IV.A. Instrumentation Development

IV.A.1. Development of a CCD Area Detector.

A charge-coupled-device (CCD) area detector for synchrotron SAXS has been tested by mounting a fiber-optic phase plate (FOPP) deposited with a thin layer (~40μ) of phosphor (Y_2O_2:Tb) in front of a CCD camera designed for high resolution visible light applications (Photometrics, Series 200). The detector, as shown in Fig. IV.A.1.1, has good linearity of response to the incident x-ray intensity and good spatial linearity (±1 per 100 pixels). The effective area on the phosphorous screen in 31.5 mm x 47.2 mm (corresponding to a (de-)magnification of 1:3.5), but can easily be adjusted (down to 1:1) by changing the distance between the phosphorous screen and the lens. The dark counts on the CCD (cooled to -25°C) is 5 counts per second, allowing up to 30 minutes of continuous measurement.

Unfortunately, the detector does not perform as well for the gain (only one out of 500 x-ray photons leads to a count), the bonding of the FOPP to the CCD is very fragile, and the "chicken wire" image of the bonded FOPP immediately in front of the CCD introduces a temperature-dependent spatial error that is difficult to correct, as shown in Fig. IV.A.1.2.

We propose to improve the detector design as follows.

i) The bonding of an FOPP to the CCD will be replaced by a quartz window some millimeters away from the CCD; so the "chicken wire" correction is no longer necessary. The new CCD chip without FOPP can be cooled down to -40°C, reducing the dark counts.

ii) The phosphorous screen will be coupled to an 18 mm image intensifier via a fiber optic taper (at a price of giving up the variable magnification of the screen); the output of the image intensifier will then be coupled to the CCD by a camera lens.

Detector Parameters

Data parameters of the CCD area detector as shown in Fig. IV.A.1.1.

Detector Size: *384 x 576 pixels, or 8.8 x 13.25 mm on the CCD; using a lens with (de-) magnification of 1:3.56 gives an active area of 31.5 mm x 47.2 mm*

Gain: *~1.3x10^{-4} (e-h) pairs ≈ 2x10^{-3} counts per x-ray photon @ 0.154 nm*

Dark Count: *~5 counts per pixel and second (CCD cooled to -25°C)*

Minimum Exposure Time: *0.1 second (shutter speed)*

Maximum Count Rate: *~1.2x10^{8} x-rays/pixel/sec*
~1.8x10^{12} x-rays/cm^{2}/sec

Detector Quantum Efficiency (DQE): *~4%, regardless of count rate*

Spatial Uniformity of Response: *+5%-20% mean, because of chicken wire; chicken wire cannot be corrected easily*

Linearity of Response vs. Intensity: *within 1%*

Spatial Resolution: *Point Spreading < 1 pixel*

Position Linearity: *±1 pixel per 100 pixels*

Other Properties: *The detector showed no measurable afterglow.*

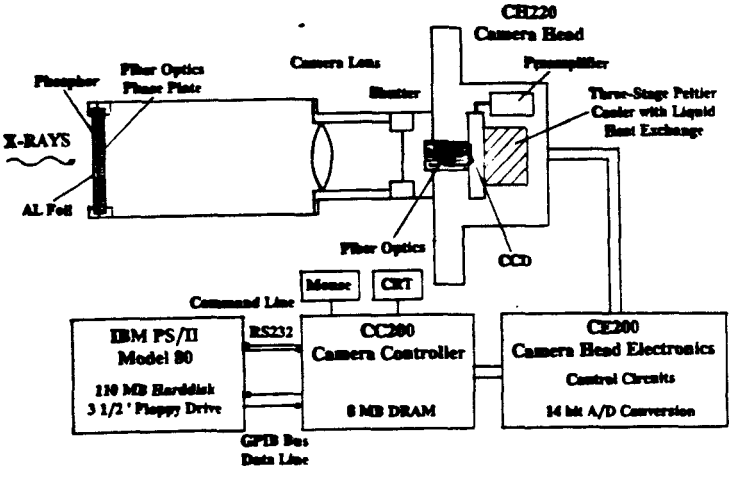

FIGURE IV.A.1.1. *CCD Detector for Synchrotron SAXS.*

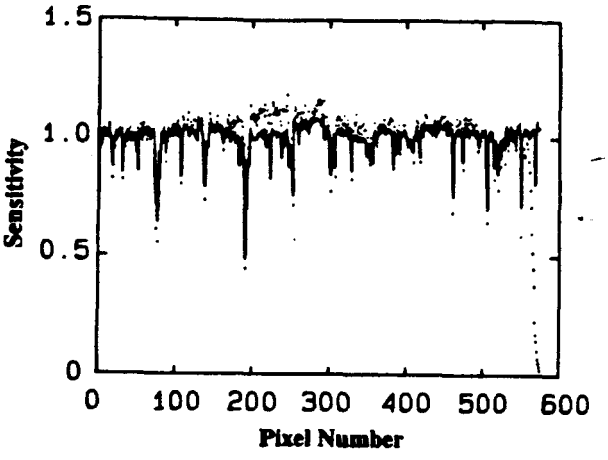

FIGURE IV.A.1.2. *The non-uniformity of response of the CCD detector to x-ray intensity. The dots show one column of a frame obtained by repeatedly scanning the detector through an x-ray source. The low sensitivity of some pixels is due to the chicken wire structure of the fiber optic phase plate bonded to the CCD. To correct for this low sensitivity one has to take a Flat Field Frame (solid line). There are three remarkable differences between the two curves:*
a) chicken wire sensitivity is lower in the image frame; e.g. flat field does not correct sufficiently.
b) in the center part the image sensitivity differs from the flat field because of differences in the thickness of the phosphor.
c) on the right side the image frame is shaded on the edge by the adapter between the lens and the fiber plate (i.e., the CCD has not been centered perfectly).

IV.A.2. Development of a Bonse-Hart Ultra-Small Angle X-ray Diffractometer (USAXD)

Essential components (θ/ϕ adjustments) for the two channel-cut crystals and the base plates have been purchased. The design is near completion. We hope to start construction of the USAXD as soon as we finalize the dimensions of the channel cut cyrstals. Some additional components and materials are required before the USAXD can be completed.

IV.B. Proposed Experiments

IV.B.1. Ionomers.

We plan to continue our collaboration with Dr. R. Lundberg at Exxon and Professor W. MacKnight at the University of Massachusetts, Amherst, on polystyrene ionomers (III.B.2). Once the X-3 A2 port has better focusing mirrors, we expect to start

our experiments on anomalous SAXS. In addition to sulfonated polystyrene ionomers, we shall continue our SAXS and ASAXS studies of poly(ethylene-methacrylic acid) (EMA) ionomers with Pb salts and PbS compounds. The lead EMA ionomers were obtained from Dr. W. Mahler at DuPont.

The work is intended to study the morphology of poly(ethylene-methacrylic acid) (EMA) ionomer Pb salts (EMA/Pb) and PbS compounds by using techniques of small angle x-ray scattering (SAXS), anomalous SAXS (ASAXS), wide angle x-ray scattering (WAXS), and differential scanning calorimetry (DSC). Preliminary experimental results suggested the presence of the ionic aggregation of the Pb groups in the amorphous region of partially crystalline matrix of EMA copolymer. An increase in Pb content in the system increased the size of the ionic aggregates and reduced, but did not eliminate, the crystalline phase. The PbS compounds were made by a reaction of Pb ionomer films with H_2S gas. In the PbS compounds, the PbS particles were present in the amorphous region and tended to aggregate and form the PbS crystallites which did not show features of the ionic structure. ASAXS could be performed at the Pb L_3 absorption edge which would permit the structural determination of pure Pb without the interference of the EMA lamellar peak. A schematic description of the ionomer structure is presented that could qualitatively explain our preliminary experimental findings.

Materials

Poly(ethylene-methacrylic acid) (EMA):

85 wt% ethylene and 15 wt% methacrylic acid

EMA/Pb Ionomers:

EMA + $Pb(Ac)_2$ -----> EMA/Pb ionomers

Pb Content (wt%):

0 (acid form), 0.2, 0.5, 1.0, 2.0, 5.0, 7.0, 10, 15, and 20

EMA/PbS Compounds:

EMA/Pb + H_2S -----> EMA/PbS

RESULTS:

Figure IV.B.1.1 shows SAXS patterns for EMA/Pb ionomers of selected Pb contents. A diffraction peak at $q \sim 0.6\ nm^{-1}$ could be observed up to 2 wt% Pb because

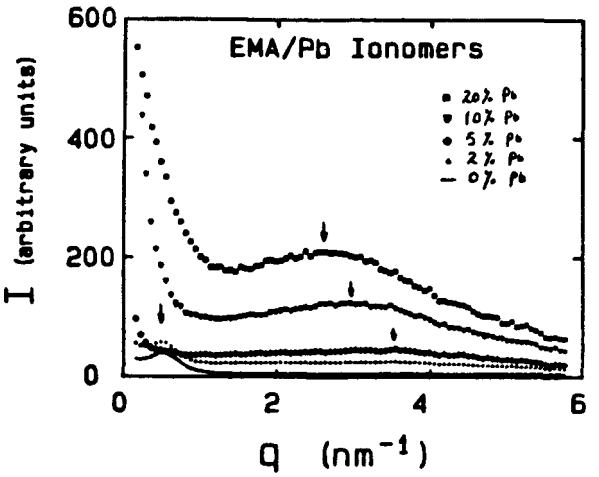

FIGURE IV.B.1.1. *SAXS patterns for EMA/Pb ionomers of selected Pb contents.*

of the lamellar structure of partially crystalline ethylene segments. This peak was becoming less sharp with increasing Pb content, and was disappeared for 5 wt% Pb sample. Another diffraction peak $2.5 \lesssim q \lesssim 3.6$ nm^{-1}, shifting to a small q and growing in peak height with increasing Pb content, could be attributed to the ionic aggregates of Pb groups. DSC showed that the crystalline phase was present for all EMA/Pb samples and the crystallinity was decreasing with increasing Pb content. Disappearance of the lamellar peak could be due to a reduction of the electron density difference between the crystalline and amorphous phases, since the Pb groups had to be in the amorphous region. The strong scattering from the ionic aggregates would overshadow the lamellar peak that might reoccur if the electron density of the amorphous phase were greater than that of the crystalline phase.

SAXS patterns for EMA/PbS compounds showed no appreciable ionic peak. A diffraction peak at $q \sim 0.6$ nm^{-1} appeared to be due to the lamellar structure. The EMA/PbS of 20 wt% Pb showed very different behavior from the others implying a different morphology. Figure IV.B.1.2 showed the SAXS patterns at small q-region. The lamellar peak was growing in height with increasing Pb content. A transition in peak shape and peak position apparently occurred at 1 wt% sample. As the Pb content increasesd, the peak position moved from $q \sim 0.6$ nm^{-1} for the sample of 0.2 wt% Pb to smaller q (~ 0.4 nm^{-1}) for that of 1 wt% Pb, then back to ~ 0.6 nm^{-1} for that of 10 wt%

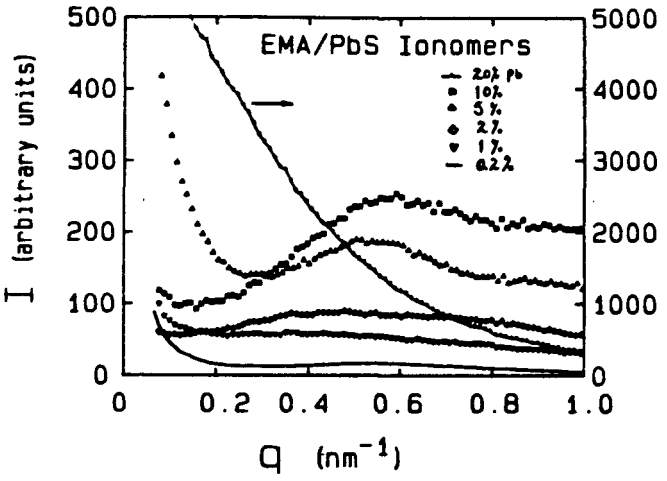

FIGURE IV.B.1.2. *SAXS patterns at small q-region for EMA/PbS compounds.*

Pb. The zeroth order scattering was much weaker than the corresponding EMA/Pb ionomers.

Figure IV.B.1.3 showed a schematic representation of EMA/Pb and EMA/PbS structures. The lamellar spacing was estimated by $d \sim 2\pi/q \sim 10$ nm with $q \sim 0.6$ nm^{-1}. The ionic aggregates were confined in a layered amorphous region so that the diameter

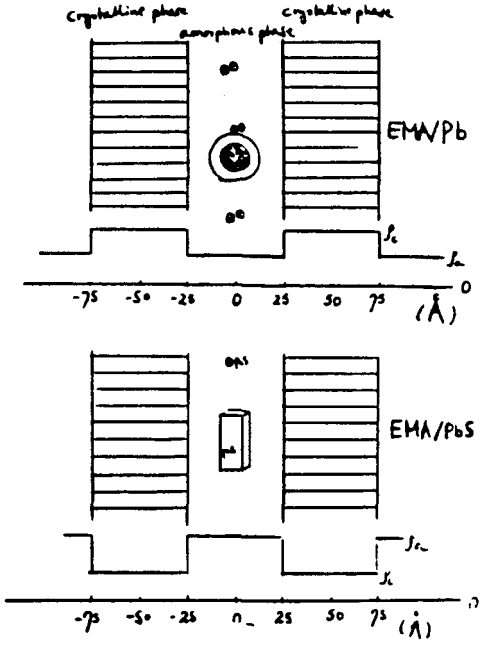

FIGURE IV.B.1.3. *Schematic representation of EMA/Pb and EMA/PbS structures.*

of a Pb aggregate was limited to a maximum of 5 nm. The aggregate size could be estimated as from ~ 1.7 nm for 0.2 wt% EMA/Pb to ~ 2.5 nm for 20 wt%.

IV.B.2. Simultaneous Small Angle and Wide Angle X-ray Scattering on Crystallization of Polyethylene Blends

The time-resolved SAXS and WAXS experiments on polymer blends are in collaboration with the research group of Professor R. S. Stein at the University of Massachusetts at Amherst. The crystallization of polyethylene blends (50/50 HDPE/LDPE and LLDPE/LDPE) will be investigated by the time-resolved small angle and wide angle x-ray scattering (SAXS and WAXS, respectively). The simultaneous measurements of the lamellar and the crystalline diffraction peaks allowed the morphological study of the PE blends in great detail during a crystallization process (quenching and slow cooling). The preliminary results for the 50/50 HDPE/LDPE (high density PE/low density PE) blend showed that during the quenching, the HD and the LD components segregated on an interlamellar scale, while during the slow cooling, the two components segregated on an inter-fibrillar scale. For the 50/50 LLDPE/LDPE blend (linear low density PE/LDPE), a similar conclusion to the HDPE/LDPE could be drawn during the slow cooling. More extensive studies will be carried out based on the preliminary findings, as shown in Fig. IV.B.2.1-3.

Small Angle X-ray Diffractometer at X3A1

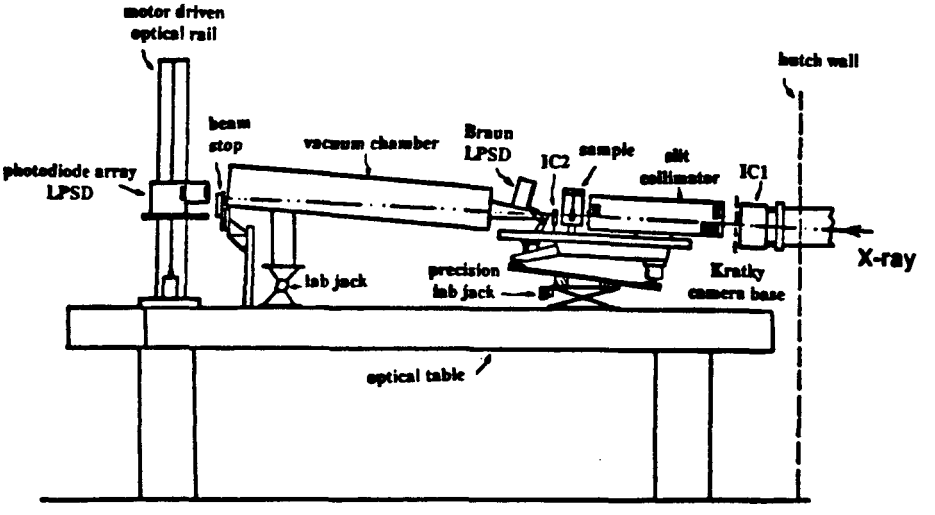

FIGURE IV.B.2.1. *Schematic diagram of the SAXD for simultaneous SAXS and WAXS measurements. A photodiode array detector (on loan from PAR; see III.A) and a Braun LPSD were used for SAXS and WAXS, respectively.*

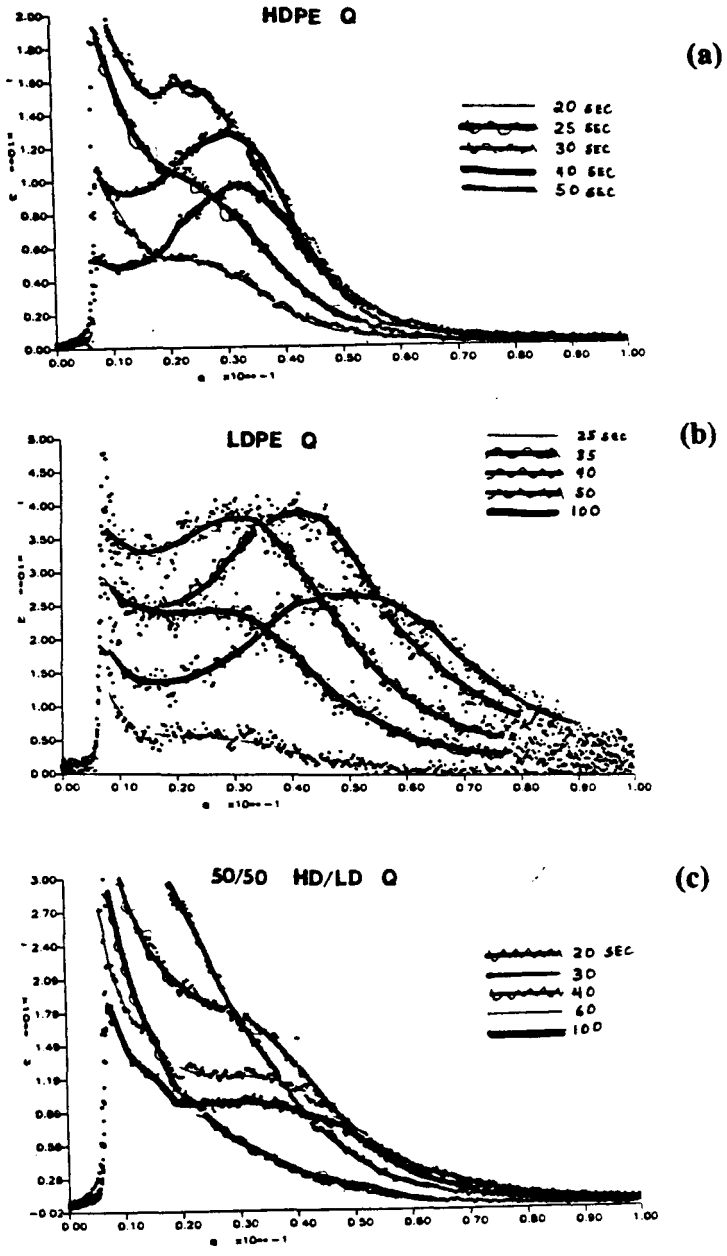

FIGURE IV.B.2.2. *SAXS patterns during the quenching process (130 °C to 60 °C) of HDPE (a), LDPE (b) and 50/50 HDPE/LDPE blend (c). No superposition of the lamellar peaks of the HD and the LD components was observed for the blend. A segregation of the HD and the LD components on an interlamellar scale was suggested. The lamellae of the HD and the LD were mixed within fibrils.*

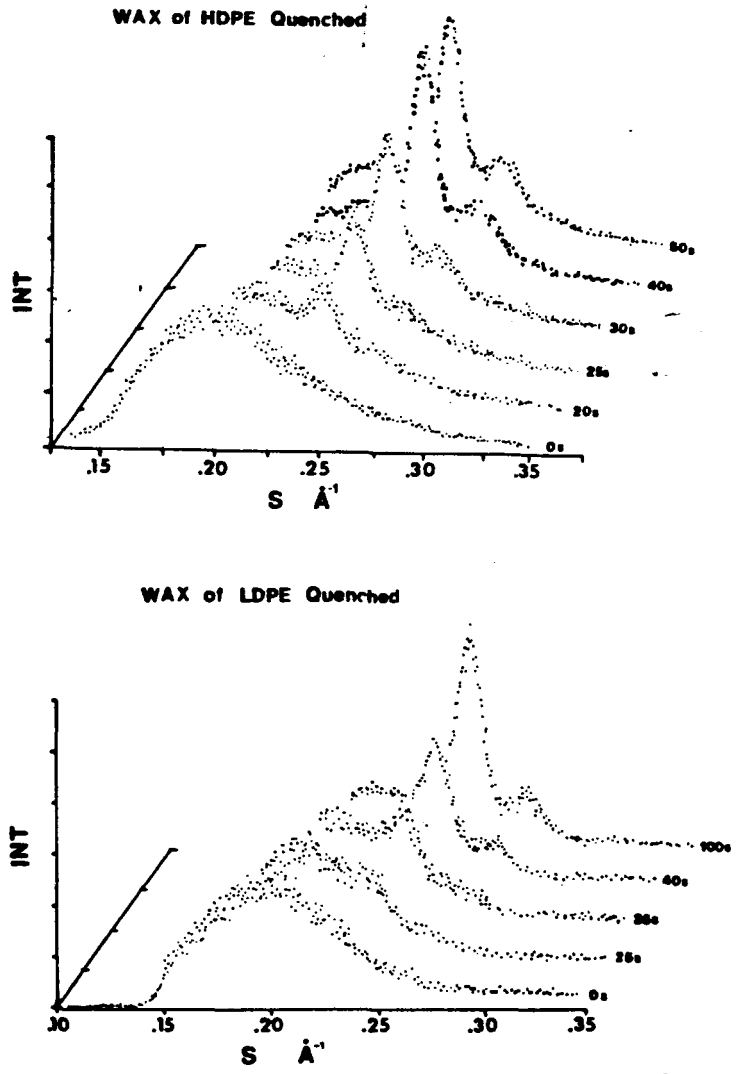

FIGURE IV.B.2.3. *WAXS patterns during the quenching (130 °C to 60 °C) of HDPE (a) and LDPE (b). The crystallinity can be obtained so that the change in density of the crystalline phase can be determined by combining the results of the invariant Q.*

Materials

	LLDPE	LDPE	HDPE
M_w	114,000	286,000	198,500
M_w/M_n	4.5	18	3.5
Short Chain Branching (per 1000 C)	18	26	-
Long Chain Branching (per M_w molecule)	-	34	-
Density (g/cm^3)	0.910	0.920	0.957